Complete single-shot measurement of arbitrary nanosecond laser pulses in time

Pamela Bowlan,[1,2*] and Rick Trebino[1,2]

[1]*Swamp Optics LLC, 6300 Powers Ferry Rd. #600-345, Atlanta, GA, 30339-2919, USA*
[2]*School of Physics, Georgia Institute of Technology, 837 State St NW, Atlanta, GA 30332, USA*
*pambowlan@gatech.edu

Abstract: For essentially all applications, laser pulses must avoid variations in their intensity and phase within a pulse and from pulse to pulse. Currently available devices work very well for both long (>10ns) and short (<100ps) pulses. But intermediate (~ns) pulses remain difficult to measure and, not surprisingly, are the least stable. Here we describe a simple, elegant, complete, all-optical, single-shot device that measures ~ns pulses and that does not require a reference pulse or assumptions about the pulse shape. It simultaneously achieves a very high spectral resolution of <1pm and a very large delay range of ~10ns (several meters of light travel). It accomplishes both goals using high-efficiency, high-finesse etalons: one to generate high angular dispersion for a high-resolution spectrometer, and another to *tilt* the pulse front by ~89.9° without distorting it in time. Using this device, we completely measure microchip and fiber-amplifier pulses.

©2011 Optical Society of America

References and links

1. J. A. Giordmaine, P. M. Rentzepis, S. L. Shapieo, and K. W. Wecht, "Two-Photon Excitation of Fluorescence By Picosecond Light Pulses," Appl. Phys. Lett. **11**(7), 216–218 (1967).
2. K. L. Sala, G. A. Kenney-Wallace, and G. E. Hall, "CW Autocorrelation Measurements of Picosecond Laser Pulses," IEEE J. Quantum Electron. **16**(9), 990–996 (1980).
3. R. Trebino, *Frequency-Resolved Optical Gating: The Measurement of Ultrashort Laser Pulses* (Kluwer Academic Publishers, Boston, 2002).
4. D. J. Kane, and R. Trebino, "Single-shot measurement of the intensity and phase of an arbitrary ultrashort pulse by using frequency-resolved optical gating," Opt. Lett. **18**(10), 823–825 (1993).
5. R. Trebino, and D. J. Kane, "Using phase retrieval to measure the intensity and phase of ultrashort pulses: frequency-resolved optical gating," J. Opt. Soc. Am. A **10**(5), 1101–1111 (1993).
6. G. Taft, A. Rundquist, M. M. Murnane, H. C. Kapteyn, K. W. Delong, R. Trebino, and I. P. Christov, "Ultrashort optical waveform measurements using frequency-resolved optical gating," Opt. Lett. **20**(7), 743–745 (1995).
7. M. Hentschel, R. Kienberger, C. Spielmann, G. A. Reider, N. Milosevic, T. Brabec, P. B. Corkum, U. Heinzmann, M. Drescher, and F. Krausz, "Attosecond metrology," Nature **414**(6863), 509–513 (2001).
8. F. Quéré, Y. Mairesse, and J. Itatani, "Temporal characterization of attosecond XUV fields," J. Mod. Opt. **52**(2), 339–360 (2005).
9. S. A. Diddams, L. Hollberg, L.-S. Ma, and L. Robertsson, "Femtosecond-laser-based optical clockwork with instability < 6.3 x 10^{-16} in 1 s," Opt. Lett. **27**(1), 58–60 (2002).
10. F. Di Teodoro, and C. D. Brooks, "1.1 MW peak-power, 7 W average-power, high-spectral-brightness, diffraction-limited pulses from a photonic crystal fiber amplifier," Opt. Lett. **30**(20), 2694–2696 (2005).
11. C. D. Brooks, and F. Di Teodoro, "Multimegawatt peak-power, single-transverse-mode operation of a 100 m core diameter, Yb-doped rodlike photonic crystal fiber amplifier," Appl. Phys. Lett. **89**(11), 111119 (2006).
12. H. Fuchs, D. Woll, T. Ulm, and J. A. L'Huillier, "High resolution FROG system for the characterization of ps laser pulses," Appl. Phys. **88**(3), 393–396 (2007).
13. J. M. Dudley, C. Finot, D. J. Richardson, and G. Millot, "Self-similarity in ultrafast nonlinear optics," Nat. Phys. **3**(9), 597–603 (2007).
14. C. Finot, G. Millot, C. Billet, and J. M. Dudley, "Experimental generation of parabolic pulses via Raman amplification in optical fiber," Opt. Express **11**(13), 1547–1552 (2003).
15. X. Gu, L. Xu, M. Kimmel, E. Zeek, P. O'Shea, A. P. Shreenath, R. Trebino, and R. S. Windeler, "Frequency-resolved optical gating and single-shot spectral measurements reveal fine structure in microstructure-fiber continuum," Opt. Lett. **27**(13), 1174–1176 (2002).

16. M. A. Foster, R. Salem, D. F. Geraghty, A. C. Turner-Foster, M. Lipson, and A. L. Gaeta, "Silicon-chip-based ultrafast optical oscilloscope," Nature **456**(7218), 81–84 (2008).
17. D. H. Broaddus, M. A. Foster, O. Kuzucu, A. C. Turner-Foster, K. W. Koch, M. Lipson, and A. L. Gaeta, "Temporal-imaging system with simple external-clock triggering," Opt. Express **18**(13), 14262–14269 (2010).
18. C. Dorrer, and I. Kang, "Linear self-referencing techiques for short-optical-pulse characterization," J. Opt. Soc. Am. B **25**(6), A1–A12 (2008).
19. C. Dorrer, and I. Kang, "Simultaneous characterization of telecommunication optical pulses and modulators by use of spectrograms," Opt. Lett. **27**, 1315–1317 (2002).
20. J. Bromage, C. Dorrer, I. A. Begishev, N. G. Usechak, and J. D. Zuegel, "Highly sensitive, single-shot characterization for pulse widths from 0.4 to 85 ps using electro-optic shearing interferometry," Opt. Lett. **31**(23), 3523–3525 (2006).
21. D. Reid, and J. Harvey, "Linear spectrograms using electrooptic modulators," IEEE Photon. Technol. Lett. **19**(8), 535–537 (2007).
22. C. Dorrer, E. M. Kosik, and I. A. Walmsley, "Direct space time-characterization of the electric fields of ultrashort optical pulses," Opt. Lett. **27**(7), 548–550 (2002).
23. F. Li, Y. Park, and J. Azaña, "Linear Characterization of Optical Pulses with Durations Ranging From the Picosecond to the Nanosecond Regime Using Ultrafast Photonic Differentiation," J. Lightwave Technol. **27**(21), 4623–4633 (2009).
24. M. Shirasaki, "Large angular dispersion by a virtually imaged phased array and its application to a wavelength demultiplexer," Opt. Lett. **21**(5), 366–368 (1996).
25. M. Born, and E. Wolf, *Principles of Optics,* 7 ed. (Cambridge University Press, New York, 1999).
26. P. Bowlan, and R. Trebino, "Extreme pulse-front tilt from an etalon," J. Opt. Soc. Am. B **27**(11), 2322–2377 (2010).
27. S. Xiao, A. M. Weiner, and C. Lin, "A dispersion law for virtually imaged phased-array spectral dispersers based on paraxial wave theory," IEEE J. Quantum Electron. **40**(4), 420–426 (2004).
28. P. O'Shea, M. Kimmel, X. Gu, and R. Trebino, "Highly simplified device for ultrashort-pulse measurement," Opt. Lett. **26**(12), 932–934 (2001).
29. R. Wyatt, and E. E. Marinero, "Versatile Single-Shot Background-Free Pulse Duration Measurement Technique for Pulses of Subnanosecond to Picosecond Duration," Appl. Phys. **25**(3), 297–301 (1981).
30. Z. Bor, B. Racz, G. Szabo, M. Hilbert, and H. A. Hazim, "Femtosecond pulse front tilt caused by angular dispersion," Opt. Eng. **32**(10), 2501–2504 (1993).
31. S. Akturk, X. Gu, P. Gabolde, and R. Trebino, "The general theory of first-order spatio-temporal distortions of Gaussian pulses and beams," Opt. Express **13**(21), 8642–8661 (2005).

1. The importance of measuring beams and pulses

Shortly after the development of the first lasers fifty years ago, researchers learned a valuable lesson: the lasers they had labored so hard to develop were not very useful if their beam spatial quality was poor. And it was. Variations in the light intensity and phase from point to point in the beam and also from pulse to pulse made experiments noisy and applications unreliable. Good beam quality—a beam with a simple spatial profile and without such fluctuations—was critical for essentially all experiments and applications. Fortunately, the naked eye can estimate beam quality in visible lasers, and cameras can more quantitatively measure it in nearly all lasers. As a result, researchers were able to improve laser-beam quality considerably. And today a key parameter of any laser's performance is its "space-bandwidth product," roughly the number of bumps in the intensity or phase vs. position (often called M^2). Lasers with a poor space-bandwidth product—a value of this parameter much greater than one—are generally of little use.

At the same time, using techniques like Q-switching and gain-switching, researchers also began to generate shorter pulses, a few nanoseconds (ns) in length. These lasers provided, not only better temporal resolution, but also much desired higher power. And just as clean, unstructured, and repeatable beams in space were important, equally important for the same reasons were analogously clean, unstructured, and repeatable pulses in *time*. The pulse *time*-bandwidth product (TBP), roughly, the number of bumps in the intensity or phase vs. *time*, is as important as its spatial counterpart in experiments and applications.

Alas, at the time, even the fastest detectors and oscilloscopes could not resolve such pulses in time. So users of ns pulses had to make do with only rough measures of them. Techniques such as autocorrelation [1, 2] emerged, involving splitting the pulse in two, crossing the two resulting pulse replicas in a two-photon absorber or second-harmonic-generation (SHG) crystal, and measuring the two-photon fluorescence or SHG intensity vs. the delay between the two pulses. Unfortunately, autocorrelation yielded only a rough

measure of the pulse length. It did not yield the pulse *shape* (the intensity vs. time); a given autocorrelation trace is consistent with many different and unknown pulse shapes. One had to assume a pulse shape even to obtain the pulse length, and, worse, the pulse phase remained entirely unknown [3]. Later improvements in autocorrelation techniques have helped but still cannot yield the intensity or phase vs. time.

In succeeding years, researchers generated ever shorter laser pulses, resulting in picosecond (ps) and eventually femtosecond (fs) pulses. But pulse *measurement* methods continued to lag behind pulse *generation* methods, and, interestingly, it was not until pulses reached fs lengths that methods emerged that could completely measure them in time. The first—and most widely used such technique today—is frequency-resolved optical gating (FROG), a spectrally resolved autocorrelation coupled with a two-dimensional phase-retrieval algorithm for retrieving the pulse [4, 5]. FROG can measure the complete pulse shape and also the phase vs. time for arbitrary fs pulses without the need for assumptions about the pulse shape or phase [3]. It is reliable, general, and convenient, and versions of it can measure even a single pulse. And it does not require a reference pulse or expensive electronics. Currently, FROGs are compact, alignment-free, self-contained and inexpensive.

As a result, fs light pulses are now arguably the best characterized type of light, even better characterized than cw light, which still requires a statistical description. FROG and other fs pulse-measurement methods have helped to take ultrafast science and technology into even shorter temporal regimes [6], including recently the attosecond regime [7, 8]. And fs lasers—now the most stable light sources ever developed—are the basis of spectacularly precise metrology applications [9].

But what about ns pulses? In pushing to ever shorter timescales, the measurement of longer—far more common—intermediate-length pulses was nearly forgotten. As a result, ns pulses from Q-switched solid-state lasers, pulsed diode lasers, and fiber lasers and amplifiers are difficult to measure. And at least partially as a result, they are usually complex in time, often varying wildly from pulse to pulse [10, 11].

Yes, ultrahigh-bandwidth oscilloscopes and light detectors have become faster and can now resolve ~100ps pulses. But such exotic electronic devices cost $100,000 or more and are complex and fragile pieces of equipment. Also, they only yield the pulse intensity vs. time. They do not measure the pulse phase vs. time and so yield only half the information in the pulse. Obtaining the phase requires heterodyning against a stable, previously measured stable reference light source at the same wavelength (which only extends the same difficult challenge to the reference light source) and measuring the beats with the same oscilloscope. Streak cameras can measure ns pulse intensities but have the same issues. Even measuring the spectra of ns pulses is unsatisfying, requiring high-resolution spectrometers and only yielding the spectrum and not the spectral phase—again only half the necessary information.

Researchers have made progress extending ultrafast measurement techniques to the ps regime and to more complex pulses. By using a large, high-resolution spectrometer, a multi-shot FROG has been demonstrated that can measure pulses up to 80 ps in length [12], and FROG measurements have been made with 20ps temporal range and sub-ps temporal resolution [13, 14]. A simple version of FROG (called GRENOUILLE) with only three easily aligned optical elements, one of which is a pentagonal SHG crystal, can measure single pulses up to ~20ps long with TBPs of up to ~20. But extending FROG to longer pulses appears impractical; the required large delay range (meters) is impractical, and the required spectral resolution is also not possible with grating spectrometers. Etalon spectrometers, which have the required resolution, are inefficient. Worse, achieving these feats on a *single shot* is even more challenging. FROG, in its cross-correlation (XFROG) variation, has been used to measure pulses with TBPs of several thousand [15], but only for pulses several ps long. And XFROG requires a previously measured reference pulse.

Several time-domain techniques based on temporal imaging can measure at least the temporal intensity of many-ps pulses [16, 17] by stretching them to many ns in length, where less expensive detectors and oscilloscopes can accurately measure their intensities vs. time. In addition, a number of linear self-referencing techniques use high-bandwidth temporal

modulators to measure pulses ~100ps long with high sensitivity [18–23]. However, these techniques require precise electronic synchronization of the pulse under test with a temporal modulator or premeasured reference pulse and so are expensive and typically operate only multi-shot and so are only useful for trains of identical pulses—an unlikely scenario for most ns lasers.

Thus, while users of exotic fs pulses have enjoyed full-characterization methods for almost two decades, the much more numerous users of more mundane ns pulses find it difficult to even perform the most basic task in their work: to measure the pulses they use.

As a result, here we present a simple nanosecond FROG. The two challenges in extending FROG—or almost any ultrafast method—to such long pulses are 1) achieving very high spectral resolution efficiently and 2) generating a many-ns delay range *on a single shot*. To meet these challenges, we use a recently developed high-efficiency etalon to achieve the necessary spectral resolution (with high efficiency). And we solve the delay-range problem in a novel manner: by *tilting the input pulse by ~89.9° without distorting it in time*. As a result, one side of a ~1cm-wide beam precedes the other by *several meters*, corresponding to ~10ns of delay. This is accomplished by focusing into another high-efficiency, high-finesse etalon [24]. Our resulting ns-FROG is also compact, robust, simple to align, and general—capable of measuring even complex pulses.

2. Frequency-Resolved Optical Gating

While FROG has defied extension to ns pulses, it is widely used for measuring pulses from a few fs to tens of ps long and has even been adapted for measuring attosecond pulses. To make a FROG measurement, the pulse is split into two replicas with a variable delay between them. They then cross in a nonlinear-optical crystal, producing a signal pulse whose brightness depends on their temporal overlap as shown in Fig. 1 (top).
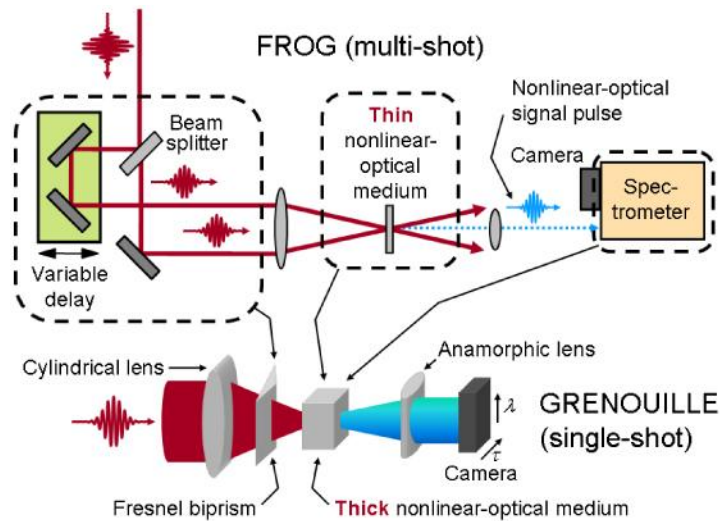
Fig. 1. A FROG is an autocorrelator followed by a spectrometer. The spectrometer spectrally resolves the signal pulse produced by the nonlinear-optical medium and yields a *spectrogram* of the pulse, which yields the complete intensity and phase vs. time. The device shown below is a simplified single-shot version of FROG, called GRENOUILLE, which replaces the beam splitter, delay line, and beam-recombining optics with a single optical component (see Fig. 2 for more details), an approach that we will also take in the device described in this article.

Second harmonic generation (SHG), which we use here, is the most commonly used optical nonlinearity, although a variety of other essentially instantaneous nonlinearities also work. But rather than measuring the energy of the nonlinear-optical signal pulse at each delay (which would yield the autocorrelation), in FROG, the signal-pulse *spectrum* at each delay is

measured. This yields the FROG trace, a spectrogram of the pulse, which is a function, not just of delay, but also of frequency, and so lives in the time-frequency domain.

Phase-retrieval algorithms based on the method of "generalized projections"—a well-known, fast, and robust algorithmic technique—extract the pulse intensity and phase, that is, its field $E(t)$ from the measured FROG trace [3]. The algorithm begins with an initial, usually random guess for the pulse's intensity and phase, which it modifies in succeeding iterations until the iterated FROG trace matches the measured one, usually in less than a second. FROG has many convenient features. For example, because the FROG trace contains more points (N^2, where N is the length of the pulse field data array) than the unknown field does ($2N$), it yields feedback that confirms the accuracy of a measurement [3].

3. High-resolution etalon spectrometer

The first challenge in measuring pulses longer than ~100ps is the spectral resolution required to resolve the SH at each delay, which, for a 3ns pulse, is ~0.2pm. Grating spectrometers cannot achieve this, so we instead use a high-resolution etalon spectrometer [24].

An etalon is simply two precisely parallel, highly reflecting surfaces, in which the output beam is the superposition of many delayed replicas of the input beam. Because the replicas experience differing numbers of round trips inside the etalon, the output wavelength varies with path length through the etalon, that is, angle; hence its angular dispersion [25]. Placing a lens after the etalon to map angle, or color, onto position at a camera yields a high-resolution spectrometer. Etalons can have as much as 100 times more angular dispersion than diffraction gratings, so sub-picometer resolution is achievable [24, 26, 27]. Because high-finesse etalons are very lossy due to their highly reflective front surface, we use an etalon with a small transparent gap on the entrance surface, reducing its loss to essentially zero. Such an etalon is often referred to as a virtual-image phase array (VIPA) [24].

4. Nanosecond pulse-front tilt from an etalon

The second—and more difficult—challenge is the generation of the required delay range of ~10ns. This can be accomplished on a multi-shot basis using a long delay line and scanning the delay over many laser shots, but this is extremely unwieldy and also requires the unknown pulse to take the form of a train of identical pulses.

A single-shot FROG measurement of *fs* pulses can be accomplished if the beams cross at an angle in the nonlinear medium (see Figs. 1 and 2a), so that one pulse precedes the other on the left side of the crystal and the other precedes the one on the right side, thus mapping delay onto transverse position at the crystal [3, 4, 28]. But for generating *ns* delays, this approach requires beams many meters in size and so is not possible. Larger delays have been achieved using tilted pulse fronts, obtained by refracting beams by a prism or diffracting beams off a grating and then crossing the oppositely tilted pulses at the nonlinear crystal (see Figs. 2b and c). This approach yields larger relative delays: for a grating, the grating's length divided by the speed of light, or 100ps for a 3cm wide grating [29]. But this approach becomes impractical for larger delays, which require beam and grating sizes of several meters.

Here we generate massive pulse-front tilt, but instead obtained from a much more dispersive optic: an etalon (see Fig. 2d), nearly identical to that used for the spectrometer. Indeed, from the Fourier-transform shift theorem, it is easy to show that, if angular dispersion (from any source) is present in a pulse, then the pulse's arrival time will vary across the beam, resulting in *pulse-front tilt* [30, 31]. In the absence of other space-time couplings, pulse-front tilt is proportional to the angular dispersion.

Propagation in the presence of angular dispersion, however, produces, in addition, other spatio-temporal distortions, including spatial dispersion—a spatial variation in the pulse's frequencies—which distorts the pulse in time. Such distortions are particularly pronounced at a *focal plane* of any lens after the etalon. Indeed, most applications of etalons specifically operate at a lens focal plane in order to use this distortion to spectrally resolve the beam. However, immediately after the angular disperser and in all *image planes* after it, spatial

dispersion is entirely absent, and the local pulse temporal shape is preserved despite the massive pulse-front tilt.
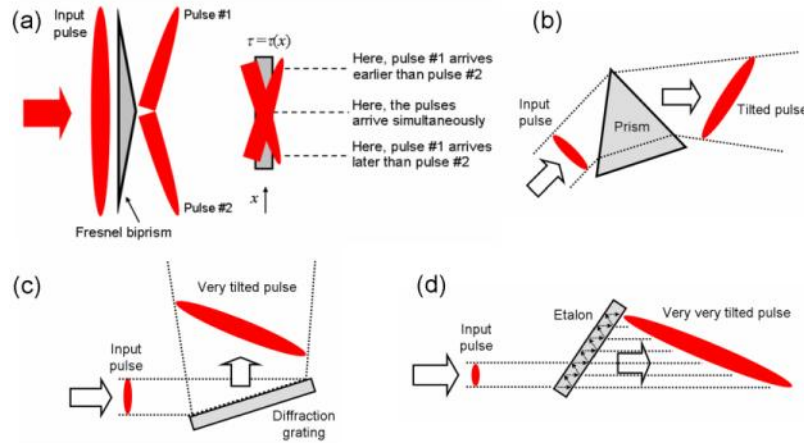
Fig. 2. a) Splitting a beam in two and crossing the resulting replicas yields a range of delays on a single shot by mapping delay onto transverse position. This can be done with a Fresnel biprism but only generates a few ps of relative delay. b,c,d) All optical elements that introduce angular dispersion also introduce pulse-front tilt. b) In prisms, because the group velocity is less than the phase velocity, the group delay is greater for rays that pass through the base of the prism than those that pass through the tip. c) In gratings, rays that impinge on the near edge of the grating emerge sooner and so precede those that must travel all the way to the far edge of the grating. d) And multiple reflections inside etalons delay the far side of the beam significantly with respect to the near side, where the beam passes directly through. While the reasons for the pulse-front tilt appear unrelated, the tilt is always proportional to the angular dispersion of the component.

Because etalons have up to 100 times the angular dispersion of a diffraction grating, their output pulse will also have 100 times more tilt, that is, nanoseconds. This can be seen by simple light-travel-time considerations: the region of the output beam that makes the most round trips through the etalon sees the most delay (see Fig. 2d). And the thicker the etalon and more reflective its surfaces, the more the dispersion and tilt. Using an interferometric technique, we recently confirmed this effect by measuring an ~89.9° tilt of a pulse emerging from a VIPA etalon [26]. A few additional (also tilted) orders (beams) emerge from the etalon, but, provided that the bandwidth of the incident pulse is less than the etalon's free spectral range, a spatial filter can remove all but one so that a single linearly tilted pulse emerges.

5. Single-shot ns-FROG

For the ns FROG, we use a simple arrangement that automatically generates two beams that cross with opposite pulse-front tilts (± ~89.9°) at the nonlinear crystal to yield the single-shot autocorrelation with a total delay range of twice the pulse-front tilt (see Fig. 3). Spectrally resolving the emerging SH then yields the FROG trace.

Specifically, a Fresnel biprism splits the input beam into two diverging pulse replicas. An anamorphic lens then redirects the beams back towards each another and also focuses each into two transparent regions on the sides of the VIPA etalon entrance face (in the horizontal direction). This lens also images the etalon onto the crystal (in the vertical direction). Two spatially overlapping, oppositely tilted pulses each spanning several ns thus emerge from the etalon and impinge on the SHG crystal, yielding a single-shot autocorrelation.

The two beams that cross in the crystal have spatial profiles consisting of an exponential decay, which, in principle, could introduce distortions into the single-shot autocorrelation, which assumes constant spatial profiles across the crystal. However, the exponential decays are in opposite directions, and their effects precisely cancel out, yielding an undistorted trace.

Three-dimensional View

(a)

Cylindrical lens (focuses into the PFT etalon)

Anamorphic lens (images PFT etalon onto crystal horizontally and focuses into crystal vertically)

Spectrometer etalon

Camera

Input pulse

Fresnel biprism (splits the beam into two)

PFT etalon

SHG Crystal

Wavelength

Delay

Anamorphic lens (images crystal horizontally and maps angle/wavelength to position vertically at camera)

Top View: Delay dimension

(b)

Pulse fronts

SHG crystal

Camera

Input pulse

PFT etalon

Delay

Fresnel biprism

Cylindrical lens

Anamorphic lens

Spectrometer etalon

Anamorphic lens

Fig. 3. a) Three-dimensional view of the ns FROG. The Fresnel biprism generates two beams, which cross (in air) and then spatially separate. The cylindrical lens redirects them toward each other and focuses them as they enter the PFT etalon. A second lens images the emerging tilted pulse fronts onto the SHG crystal, where relative delay of the two pulses is mapped onto transverse position. The SHG crystal performs the single-shot autocorrelation and is imaged onto the camera's horizontal dimension. Simultaneously, the beam is spectrally resolved along the vertical dimension by an etalon spectrometer (a VIPA etalon followed by a focusing lens), resulting in a single-shot FROG trace at the camera. b) Top view of the single-shot ns-FROG. Not shown: a filter that absorbs the input pulse but transmits the second harmonic and slit at the focal plane of the imaging lens that removes the higher orders from the etalon. In our experiments, we used two cylindrical lenses rather than anamorphic lenses.

The SH beam is then spectrally resolved at each delay, using an imaging VIPA-etalon spectrometer, yielding the SHG FROG trace at the camera. To do this, the green beam out of the SHG crystal is focused vertically into the gap of the spectrometer-etalon input face. Then another anamorphic lens, located its vertical focal length away from the camera, maps angle, or color, onto the camera's vertical dimension, and, in the horizontal dimension, it images the SHG crystal onto the camera's horizontal, or delay, axis.

In our experiments, the two-gap pulse-front tilt etalon was a solid-glass etalon with front and back reflectivities of 97% and 99.3%, respectively, at 1064nm. This etalon was square with an aperture size of 30 by 25 mm and the two gaps on the front surface were 5 by 25 mm. The etalon's thickness was 1cm, corresponding to a free spectral range of 34pm or 10.6GHz, and experimentally we found its line width to be ~0.9pm or 954MHz, or a finesse of 42. From light-travel time considerations, this results in delay range of 8.4ns between the two oppositely tilted pulses. The Fresnel biprism had an apex angle of 160°. A 120mm focal-length cylindrical lens was placed at a distance slightly greater than its focal length after the biprism to focus the two beams into the two gaps of the etalon with an incident angle of ~1° with respect to the etalon's normal. Rather than the anamorphic lens shown in Fig. 3a, we used two cylindrical lenses having focal lengths of 200mm and 100mm before the SHG crystal. Due to its high nonlinearity at 1064nm, we used a 1cm-thick $LiIO_3$ SHG crystal.

Our spectrometer etalon was also a solid piece of glass with 97% front and 99.3% back surface reflectivities and with a 3mm high transparent gap at the bottom of the front surface.

Its width was 1cm (free spectral range = 10pm). We tilt it at an angle 0.9° with respect to the incoming beam. We experimentally found its line width to be 0.13pm (138 MHz).

6. Measurements

We tested the ns FROG using both a Nd:LSB microdisk laser from Standa and also amplified pulses resulting from a master-oscillator fiber-amplifier (MOFA), the set up for which was very similar to the first amplification stage in reference [10]. The microdisk laser was diode-pumped and emitted slightly sub-nanosecond pulses at 1064nm with ~8μJ of energy and a 10kHz repetition rate. We amplified these pulses with a one-stage Yb fiber amplifier that was 2m-long, polarization-maintaining, and had an inner-core diameter of 25μm and an outer-core diameter of 250μm. We coiled the fiber to achieve single-mode operation. For the amplifier pump, we used a 976nm diode laser, which we free-space-coupled to the fiber. We chose this system in part because, unlike most ns lasers, it is relatively stable from pulse to pulse, facilitating our FROG's first phase of development. On the other hand, it provided a different challenge in that its μJ pulse energy was significantly less than, say, a typical Q-switched laser (~mJ).

In all of our measured FROG traces, we used a grid size of 128 × 128. Finally, to retrieve the pulse's field $E(t)$ from the FROG trace, we used the same widely available program as for femtosecond FROG traces described above.
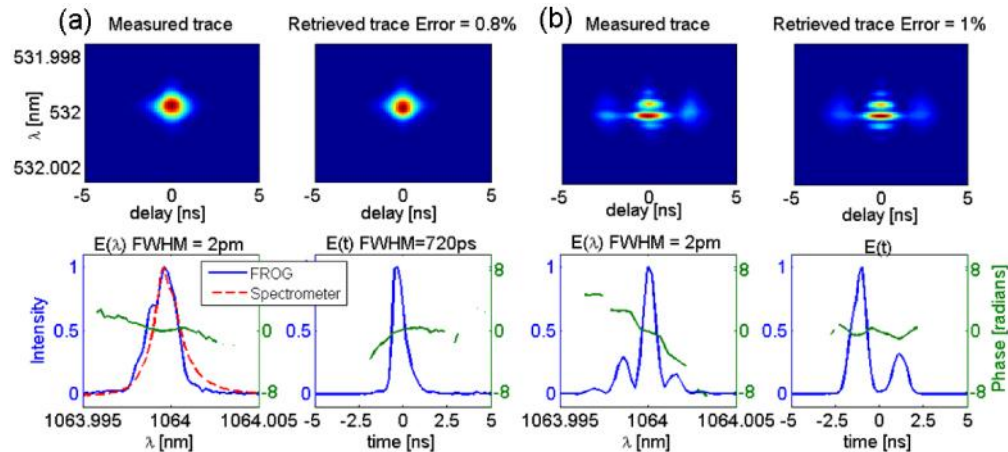
Fig. 4. Testing the FROG: (a) FROG measurement results for the output of a 1064nm microdisk laser. The spectrum shown in red was measured with a VIPA etalon spectrometer for comparison with the FROG results. (b) FROG measurements of a 2.6ns double pulse generated by sending the pulses from the microdisk laser through a Michelson interferometer in which one arm was 39cm longer than the other. A 36% relative intensity of the two pulses was expected and also correctly measured by the FROG. Note that all of the figures in the top row share the same y-axis. In both of these measurements, we averaged over ~100 laser pulses due to the low pulse energy.

Figure 4a shows the measured and retrieved traces and intensities and phases in the time and frequency domains for the pulse from our microdisk seed laser (see Fig. 4a), yielding a slightly chirped 720ps pulse with a bandwidth of ~2pm. To confirm this result, we made an independent measurement of the laser's spectrum using a VIPA etalon spectrometer for 1064nm (with 0.9pm resolution), and these two spectra are in reasonable agreement.

A much better test of the ns FROG is a double pulse from an unbalanced Michelson interferometer because it has a very distinct and characteristic FROG trace (see Fig. 4b top). In addition, such a trace can also be used to calibrate the delay and frequency axes, given the path-length difference in the Michelson interferometer (which can be measured in this case simply by using a ruler). Our Michelson interferometer yielded two pulses with a 2.6ns pulse separation and whose relative intensity we measured to be 36% (using a power meter). This pulse provides an excellent test for another reason: it is quite complicated, having a FROG-

trace spectral fringe spacing of 0.36pm and a time bandwidth product of ~15. The measured FROG trace and retrieved pulse for this double pulse are shown in Fig. 4b. Note the expected oscillations in the measured spectrum—the nature of a double-pulse spectrum. These measurements nicely illustrate the ~8ns of delay range and sub-picometer spectral resolution of our FROG. (Also, note that the individual measured pulse in Fig. 4a appears to be the time-reversed replica of the actual pulse, as revealed by the pulses in Fig. 4b, where we know that the weaker pulse was second. This is the well-known, but trivial, direction-of-time ambiguity in SHG FROG, which is easily removed, as we have done here.)

   The ns FROG is a useful tool for watching both the time- and frequency-domain structure of the pulse evolve in real time as, say, amplifier pump power is varied, particularly important in amplified systems, such as ours. Due to stimulated Brillouin scattering and self-phase modulation, the spectrum broadens and red-shifts as the amplified seed pulse gains more energy (see Fig. 5). Figure 5a shows the measured ns FROG trace for different amplifier pump power levels.
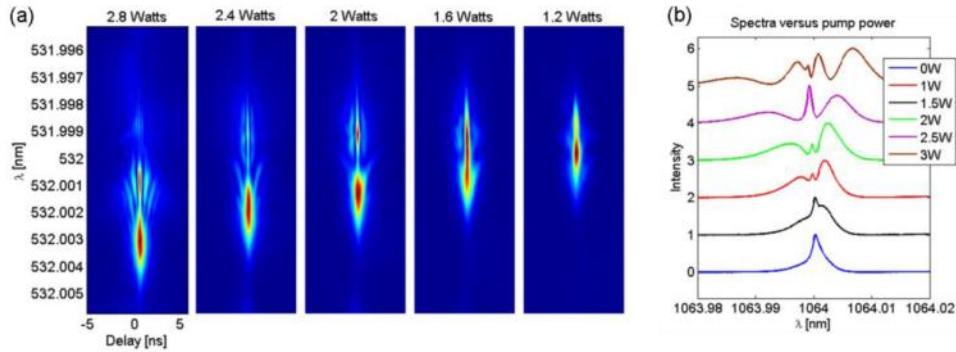
Fig. 5. FROG and high-resolution spectral measurements of amplified pulses: (a) FROG traces of pulses from the Yb-fiber amplifier for different pump power levels. (b) Spectra of the amplified pulses versus pump power using the 1064nm VIPA etalon spectrometer. In these FROG traces we averaged over ~100 pulses.

   Figure 6 shows our ns-FROG measurements of amplified pulses using amplifier pump power levels of 2 and 2.8Watts, and independent VIPA spectrometer measurements are shown in red for comparison. The pulses shown in Fig. 6a and b were amplified by $12 \times$ and $15 \times$, resulting in an average power of 170mW and 213mW.
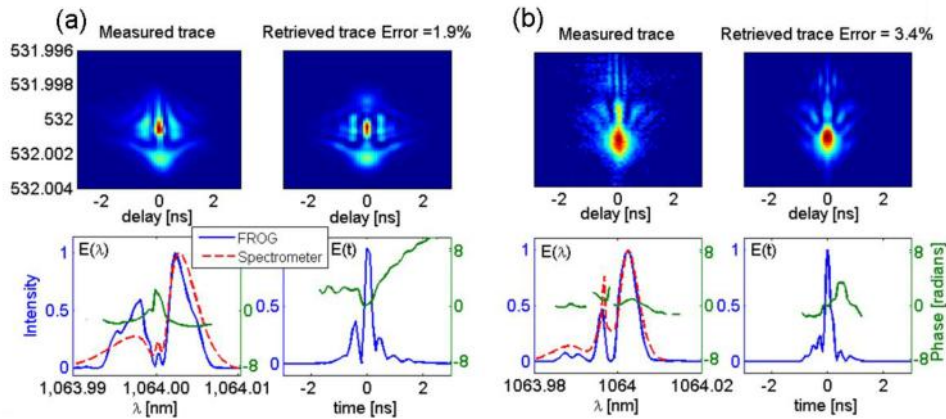
Fig. 6. Measurements of amplified pulses. FROG results for $12 \times$ (a) and $15 \times$ amplification (b). The results shown at right were a measurement of a single pulse, and in the left we averaged over ~100 pulses.

Due to low pulse energy from our laser/amplifier set up, all of the previously described measurements were averaged over ~100 pulses. With more amplification, however, we were able to make true single-pulse measurements and, for example, confirm that the amplified pulse's temporal intensity and phase were not varying from shot-to-shot. This is the case for the results shown in Fig. 6b, where the energy of a single pulse was slightly above our single-shot detection level. The higher error in that measurement is due to the higher noise in the trace due to the low signal level (after standard noise filtering). Most ns lasers have higher power than our fiber laser set up, so single-shot measurements for them using the ns Frog should be straightforward and low-noise.

Finally, we mention that, in the results shown in Fig. 6a and b, the FROG spectra are slightly different from those measured with spectrometers. These differences are likely because all the spectrometers in these measurements were at their limits of spectral resolution. and spectral structure is slightly washed out in them all by varying degrees. Thicker etalons would resolve this issue and should be used in future devices for measuring such pulses.

7. Discussion

The measurements above demonstrate our single-shot FROG's ability to measure even complex pulses in the 175ps to 3ns range, using a very simple, all-optical device. The table below summarizes the parameters of our ns FROG.

Table 1. Summary of the parameters of the ns-FROG used here.

Spectral Resolution	Spectral Range	Temporal Resolution	Temporal Range	Maximum TBP	Measurable pulses at 1064nm
0.37pm (~4ns)	27pm (~60ps)	13ps Or 60ps	8.5ns Or 1.8ns	~30	130ps to 4ns or 60ps to 1.8ns

In addition to the previously mentioned issues, the measurement range of our ns FROG is also limited somewhat by the need to image through the spectrometer etalon. Because there is a large optical path-length difference between the light that exits the etalon on the first and last bounces, a large *depth of field*, equal to this distance, is required. Given the required depth of field of ~1.5m (the pulse-front tilt), we can solve for the smallest resolvable feature, which we find to be ~350μm. Our SHG crystal had a width of 2mm along the delay axis. So by choosing the correct imaging lenses, ~30 temporal features can fit across the crystal and be accurately imaged through the 532nm etalon. Therefore, the maximum measurable TBP of our device was ~30. This is the reason for the two options in the above table.

The next limitation in measurable pulse complexity is given by the finesse of the SHG spectrometer etalon, which is ~90 for our current setup. Of course, the FROG could also measure broader- or narrower-bandwidth pulses simply by using narrower or thicker etalons.

The single-shot ns FROG should work for a large range of center wavelengths, with the bandwidth of the etalon's coatings providing the only limitation in this regard. A different center wavelength simply changes the output angle of the tilted pulse from the PFT etalon, much as the diffracted angle from a grating would change. But because we image the etalon onto the SHG crystal, angle changes will not affect the alignment of the FROG, although the slit may need adjusting. Changes in the input pulse center wavelength should simply move the FROG trace up and down along the wavelength axis and may require tilting the SH crystal to maintain the phase matching angle.

In short, this simple and inexpensive device should prove an essential accessory in ns laser labs. It will allow users and laser developers to monitor the performance of their ns lasers on a shot-by-shot basis and provide the information required to vastly improve the most numerous and popular class of lasers in the world.

Acknowledgements